

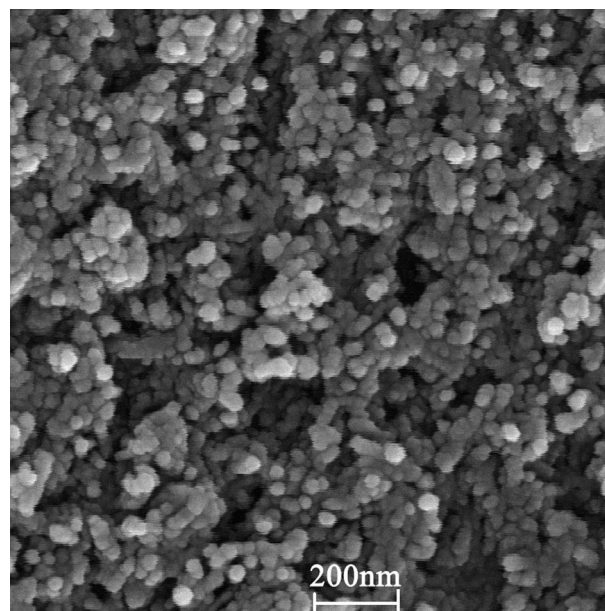
Green synthesis of zirconia nanoparticles using the modified Pechini method and characterization of its optical and electrical properties

Ali Majedi¹ · Alireza Abbasi¹ · Fatemeh Davar²

Received: 11 March 2015 / Accepted: 30 September 2015 / Published online: 20 October 2015
© Springer Science+Business Media New York 2015

Abstract Zirconia nanoparticles with the cubic phase were prepared from zirconium acetate and lemon juice as the precursors. Then, the effect of sucrose addition on improving the particle size and the agglomeration of product was investigated. The particle size of as-synthesized nanoparticles was obtained using FESEM. The results showed that the as-obtained product with the mix of lemon juice (20 mL) and sucrose had a better morphology with the mean particle size of about 21 nm. These nanoparticles were selected and further characterized by EDS, AAS, XRD, UV–Vis, and PL spectroscopy. The EDS and AAS revealed the presence of Mg and Ca in the sample introduced from lemon juice. Also, XRD confirmed the formation of the cubic-phase zirconia. The synthesized cubic ZrO₂ nanoparticles exhibited a broad photoluminescence in the UV–Vis region. Then, a pellet from these nanoparticles was prepared and the electrical property of this sample was measured in the temperature range of 450–750 °C using four-probe techniques. The results revealed that these zirconia nanoparticles could have a potential application as an electrolyte material in the intermediate-temperature solid oxide fuel cells.

Graphical Abstract



Keywords Stabilized zirconia · Nanoparticles · Lemon juice · Sucrose · Photoluminescence · Fuel cells

1 Introduction

ZrO₂ is a ceramic material with a number of interesting and useful properties [1]. It exists in three crystal phases [2]. At atmospheric pressure, the monoclinic (m) phase is thermodynamically stable at room temperature, the tetragonal (t) phase exists in the temperature range of 1100–2370 °C, and the cubic (c) phase is found above 2370 °C [3]. When

✉ Fatemeh Davar
davar@cc.iut.ac.ir

¹ School of Chemistry, College of Science, University of Tehran, Tehran, I. R. Iran

² Faculty of Chemistry, Isfahan University of Technology, Isfahan, I. R. Iran

it is used at the elevated temperature and then cooled to the room temperature, the volume expansion occurs from cubic to tetragonal, subsequently leading to monoclinic transformation. These volume changes induce large stresses causing the crack. Thus, the bulk zirconia cannot be used at elevated temperatures due to this volume change [4]. Therefore, more attention has been given to stabilizing the cubic and/or tetragonal phase of zirconia at the room temperature. Generally, two approaches are used for this purpose. The first one is based on the nanocrystallization of zirconia particles that lower the surface energy for the tetragonal and cubic phases, rather than the monoclinic one. It was estimated that, based on surface energy effects, the critical size for the stabilization of the tetragonal phase was about 30 nm [5]. In the second approach, a small amount of metal oxides such as MgO [6], CaO [7], and Y_2O_3 [8] is doped in the zirconia lattice. The metal oxides ions substitute some of the zirconium ions in the crystal lattice, thereby causing the stabilization of these phases at the room temperature. These additives “adjust” the crystallographic structure by introducing oxygen vacancies and altering the electronic structure. Generally, it is these modifications, i.e., the vacancies and the changes in the geometric and electronic structure, which lead to the useful transport as well as the chemical and optical properties of the doped ZrO_2 [9]. Over the past several years, a number of techniques have been developed for the production of zirconia nanoparticles, including physical and chemical methods such as laser ablation [10], microwave plasma [11], thermal decomposition [12], hydrothermal techniques [13], and sol–gel methods [14]. The sol–gel process is one of the most widely utilized methods for the preparation of doped and pure nanocrystalline ZrO_2 [5, 15–17]. The sol–gel process has unique advantages such as the mild reaction conditions, good control over the structure and kinetics of the process, and the fine control of the product’s chemical composition, which is especially suitable for preparing multicomponent materials and enabling small quantities of dopants to be introduced in the sol such that it can be ultimately dispersed in the final product uniformly [18]. Despite these advantages, the sol–gel method used for the preparation of ZrO_2 utilizes zirconium(IV) alkoxides as a precursor which suffers from high cost, unavailability, toxicity, and fast hydrolysis rate (thereby making it difficult to control the homogeneity of different components during the experimental processes) [19]. These disadvantages can be notably prevented by a Pechini-type sol–gel process that makes use of cheaper precursors. The Pechini-type sol–gel process (also known as the polymerizable complex technique) includes a combined process of metal complex formation and in situ polymerization. It is based on the fact that certain α -hydroxycarboxylic organic acids such as citric acid (CA) can form stable chelates with several

cations, and their polyesterification with a polyhydroxy alcohol such as ethylene glycol (EG) makes a polymeric resin. The immobilization of metal cations in such a highly branched polymer can prevent, or at least reduce, the cation mobility during the heat treatment, causing the formation of nanoparticles [20]. However, this method also suffers from particles agglomeration [21]. Biological methods using plant extracts and microorganisms have been proposed as alternative environmentally friendly methods in the synthesis of nanosized materials [22]. Biomolecules can function as stabilizers and capping agents controlling the crystal growth [23]. In this study, we have reported on the facile synthesis and characterization of cubic ZrO_2 nanoparticles with lemon juice extraction. In addition, sucrose was applied to obtain less agglomerates. It is known that sucrose and lemon juice are cheap, non-toxic, available at industrial scale, and easy to store and manipulate at low temperatures. The particle size of as-produced particles was obtained with the aid of FESEM. The more uniform and smaller size particle was chosen for EDS, AAS, XRD, UV–Vis, and PL analysis. The electrical conductivity test of it was investigated too.

2 Experimental

2.1 Materials and methods

Lemon fruits (*Citrus aurantifolia*) purchased from a local market were peeled and squeezed. The resultant pulps were then filtered using muslin cloth to remove the solid particles. The pH value of the solution was between 3.7 and 4.0. Then, 250 mg zirconium(IV) acetate was dissolved in 20 mL ethylene glycol and the extracted lemon juice in different volumes of 10, 20, and 30 mL was added slowly under stirring condition in 1 h. The mixtures were heated to 90 °C under continuous stirring for 3 h; after that, the brown gel was observed. The gel was calcined at 750 °C for 2 h. In another experiment, 1 g sucrose was dissolved in the extracted lemon juice and other steps were repeated as mentioned above. For comparison, 250 mg zirconium(IV) acetate was dissolved in 20 mL ethylene glycol and 20 mL distilled water was added and other steps were repeated again. The samples were cleaned with deionized water and ethanol prior to characterization. The synthesized samples were analyzed by field emission scanning electron microscopy (FESEM, Tescan mira, Czech). The XRD patterns were recorded on a Philips X’pert Pro MPD model X-ray diffractometer using $Cu K_{\alpha}$ radiation as the X-ray source. The diffractograms were recorded in the 2θ range of 20°–80°. The UV–Vis absorbance spectra were obtained for the samples using spectra UV–Vis double-beam PC scanning spectrophotometer

model UVD-2950 equipped with a glass of 1-cm path length; furthermore, the spectra were recorded at room temperature in air within the range of 200–600 nm. Moreover, for comparison optical properties of nanosized zirconia with bulk sample, the one sample was prepared with Pulse Electrical Explosion (PEE) Nano Engineering and Manufacturing Co. (Model: PEE10k or PEE50K (Nano Engineering and Manufacturing Co. (PNF Co.), made in Iran). The PL spectroscopy was used with the xenon light at 210 nm. We measured the density of the sintered samples using Archimedes' method in distilled water.

2.2 Sintering and conductivity measurements

For electrical conduction measurement, zirconia nanoparticles synthesized by 20 mL lemon juice and sucrose were selected. The cubic pellets with the dimensions of 3×2.5 mm in surface and 2.1 mm in thickness were prepared by the uniaxial pressure of the mixed powders at 400 MPa for 1 min. After that, the specimens were sintered in air in different temperatures for 4 h. Four-probe conductivity measurement was taken on the selected specimen. High-temperature silver paste was applied on both sides of the pellets to make the electrodes. After drying the pasted silver electrode, the pellets were again sintered to the temperature of 500 °C with 5 °C raise per min from room temperature and kept at 500 °C for 2 h and then cooled to room temperature.

3 Results and discussion

3.1 FESEM and EDS analysis of synthesized powders

Figure 1 shows the FESEM micrographs of as-synthesized ZrO_2 particles. From Fig. 1a, it could be seen that the sample synthesized without the use of any modifier (lemon juice and sucrose) had an agglomerated and a micron-size structure. Citric acid is known as the predominant organic acid component in lemon juice, and its amount ranges from 5 to 6 % [24]. So, it could be applied as α -hydroxycarboxylic acid in the Pechini-type sol-gel process. By using lemon juice with the volume of 10 mL, it was observed that the size of ZrO_2 particles became smaller (Fig. 1b). The smallest nanoparticles were formed using 20 mL lemon juice (Fig. 1c). However, it was notable that the particles were merged together and embedded in the adjacent particles (agglomerated particles). This agglomeration was increased with more lemon juice usage (Fig. 1d). Figure 1e, f shows that with the addition of sucrose to the starting material, the uniformity of the

products was improved. According to Fig. 1, the sample prepared with 20 mL lemon juice and sucrose (Fig. 1e) had the smaller particle size of 21 nm as compared to other samples. Thus, this sample was used for further analysis. The EDS data of ZrO_2 synthesized by 20 mL lemon juice and sucrose are shown in Fig. 2. Nano- ZrO_2 showed characteristic peak lines around 0.18, 2.04, and 15.74 keV, which could be attributed to M_{α} , L_{α} , and K_{α} for Zr and 0.52 keV for K_{α} of O, respectively. Moreover, the EDS data of the sample showed characteristic emission lines of 1.25 keV of Mg K_{α} and 3.69 keV of Ca K_{α} [25]. Lemon juice contains some minerals such as Ca^{2+} and Mg^{2+} [24]. It could be, therefore, concluded that Ca and Mg were entered in the ZrO_2 structure from lemon juice. As implied in the introduction, there have been a lot of studies doping ZrO_2 with Ca^{+2} , Mg^{+2} , and other cations. With doping these compounds, the cubic phase of zirconia could be stabilized at room temperature.

3.2 Composition analysis

To determine the composition of Ca and Mg in the synthesized nanoparticles, first, 100 mg of zirconia powder was dissolved in 10 mL aqua regia solution for 24 h. Then, Ca and Mg contents of the prepared solution were measured by atomic absorption spectroscopy. 2.673 mg Ca and 1.756 mg Mg were detected by AAS per 100 mg of nanoparticles powder synthesized by 20 mL lemon juice and sucrose.

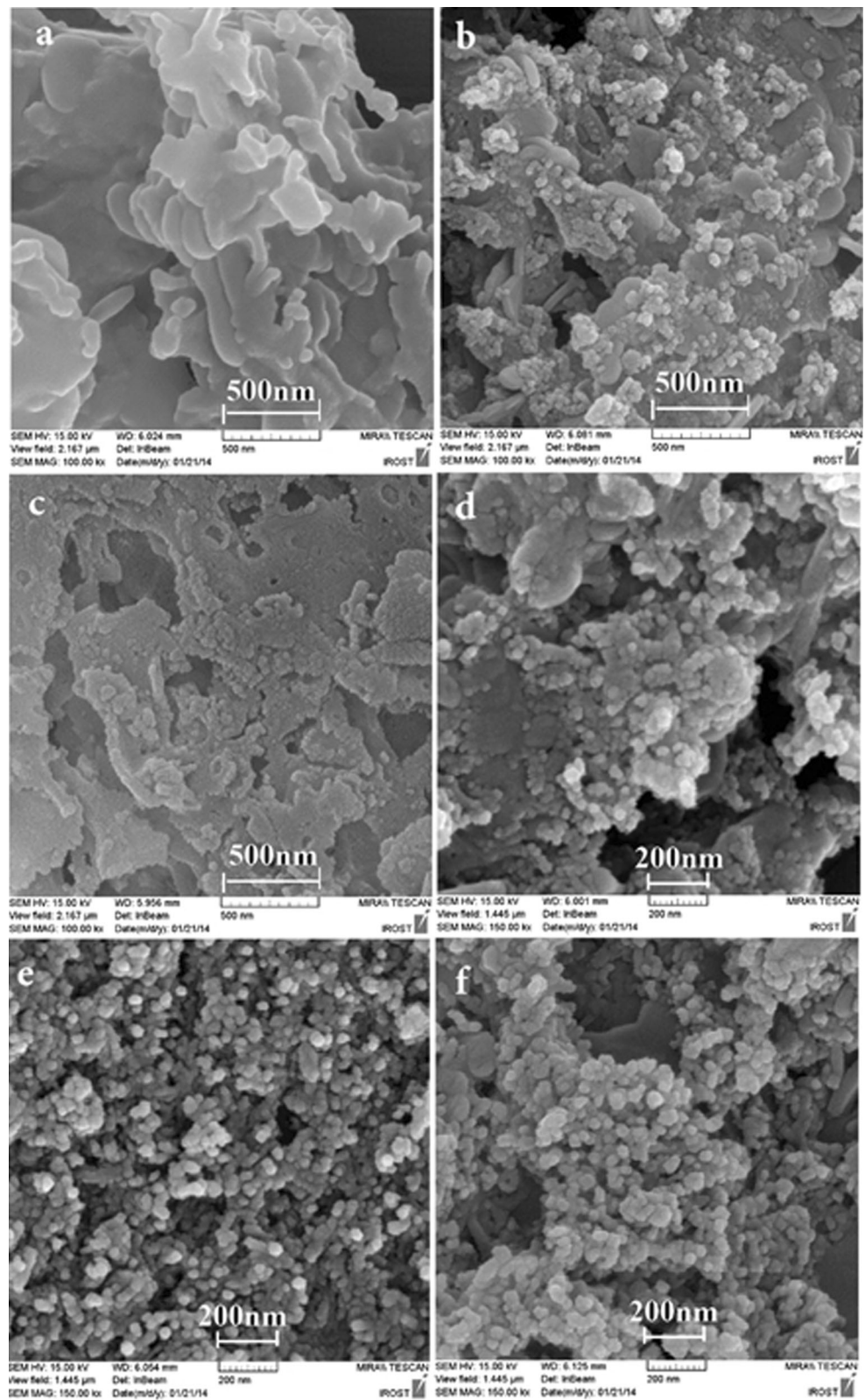
3.3 TG-DTA investigation

The TGA curve for the decomposition TG-DTA curve of the zirconia gel was prepared using sucrose and 20 mL lemon juice, as shown in Fig. 3. A little weight loss could be observed in the range of 100–250 °C, probably due to dehydration. An exothermic peak of about 350 °C was followed by a weight loss of about 40 wt%, between 250 and 700 °C. This could be attributed to the oxidation and the decomposition of organic compounds such as polyester in the sample [26].

3.4 FT-IR Analysis

The IR spectra of the uncalcined gel and the synthesized nanoparticles calcined at 750 °C are shown in Fig. 4. The gel and calcined samples exhibited –OH stretching vibration in the frequency range of 3136–3857 cm^{-1} . The reduced reflectance and the bond depth of the gel powder could be ascribed to the non-crystalline nature of the material [27]. The band peaks 1637 and 1726 could be due to the carbonyl groups of a carboxylic acid and an ester, respectively. This confirmed that both carboxylic acid

Fig. 1 FESEM images of synthesized ZrO_2 : **a** without the use of any modifier; **b–d** with the use of only lemon juice in the volume of: **b** 10 mL, **c** 20 mL, and **d** 30 mL; and **e, f** through the use of sucrose and lemon juice in the volume of: **e** 20 mL and **f** 30 mL



(unreacted citric acid of lemon juice) and ester groups (which resulted from the reaction of CA and EG molecules) existed in the obtained uncalcined gel. These peaks

disappeared in the heat-treated sample. In the calcined sample, new bands observed at 499 and 580 cm^{-1} corresponded to $Zr-O$ vibrations. Also, $M-OH$ stretching and

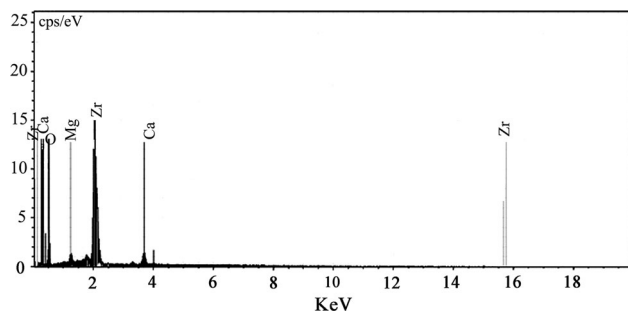


Fig. 2 EDS spectrum of ZrO_2 synthesized by 20 mL lemon juice and sucrose

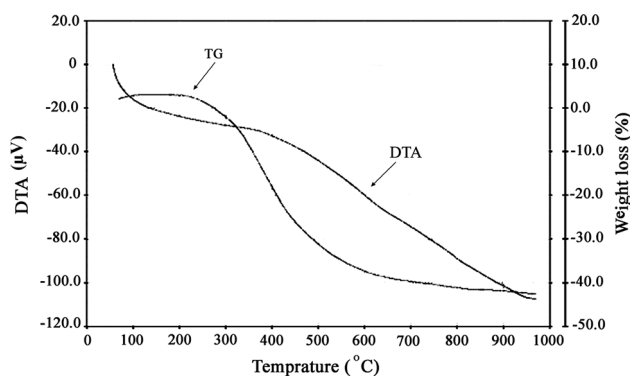


Fig. 3 TG–DTA curve of gel prepared using sucrose and 20 mL lemon juice

the bending vibration of structural water, M–OH bonding, could be seen at 1036 cm^{-1} [28].

3.5 XRD analysis

The XRD pattern of ZrO_2 nanoparticles synthesized by 20 mL lemon juice and sucrose is shown in Fig. 5. The XRD pattern demonstrated that the product had a cube phase (JCPDS card No. 27-0997). The broadening XRD peak showed that the crystallite size of ZrO_2 was fine. Calculated via the Scherrer formula [24], the average crystalline size for ZrO_2 sample was about 20 nm. Moreover, as compared to the reference pattern, a slight shift to higher or smaller d-values was seen. These shifts could be attributed to a distortion in the unit cell structure. The XRD pattern did not show any magnesium or calcium phase, and therefore, it could be concluded that Mg and Ca were doped into the structure of zirconia, thereby leading to this distortion in the zirconia unit cell.

According to Pechini method, the first step in making nanoparticles is the preparation of stable metal chelate complexes such as Zr–citric acid of lemon juice (CA complexes). It is known that most zirconium–CA complexes are soluble and stable in a mixed solvent of EG and

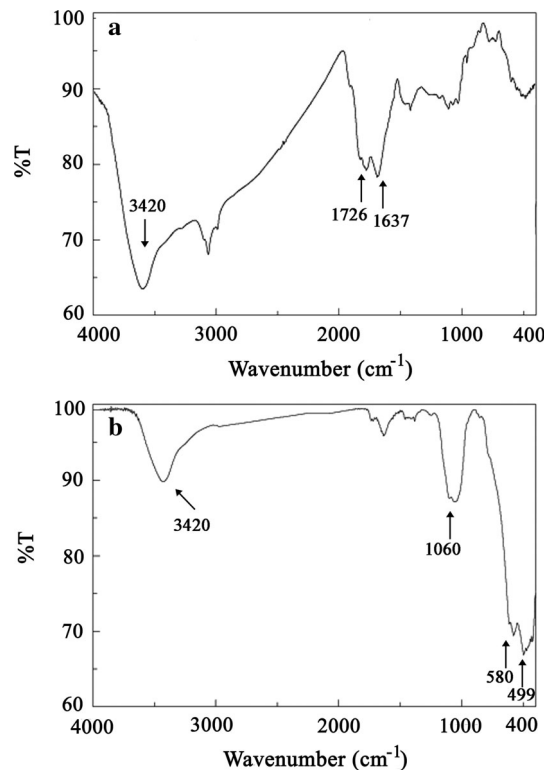


Fig. 4 FT-IR curves of synthesized ZrO_2 : **a** dried gel and **b** calcined at $750\text{ }^\circ\text{C}$

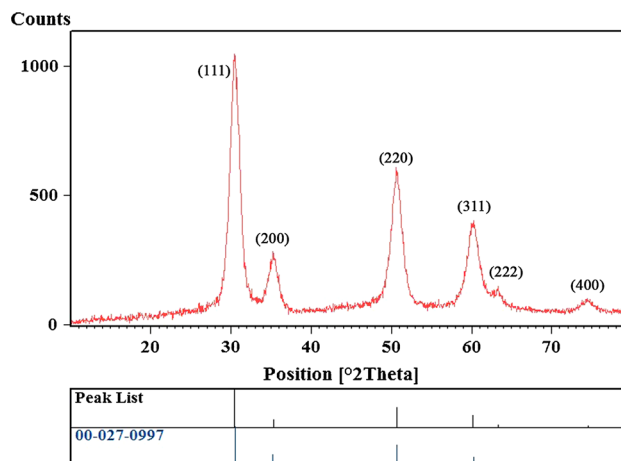
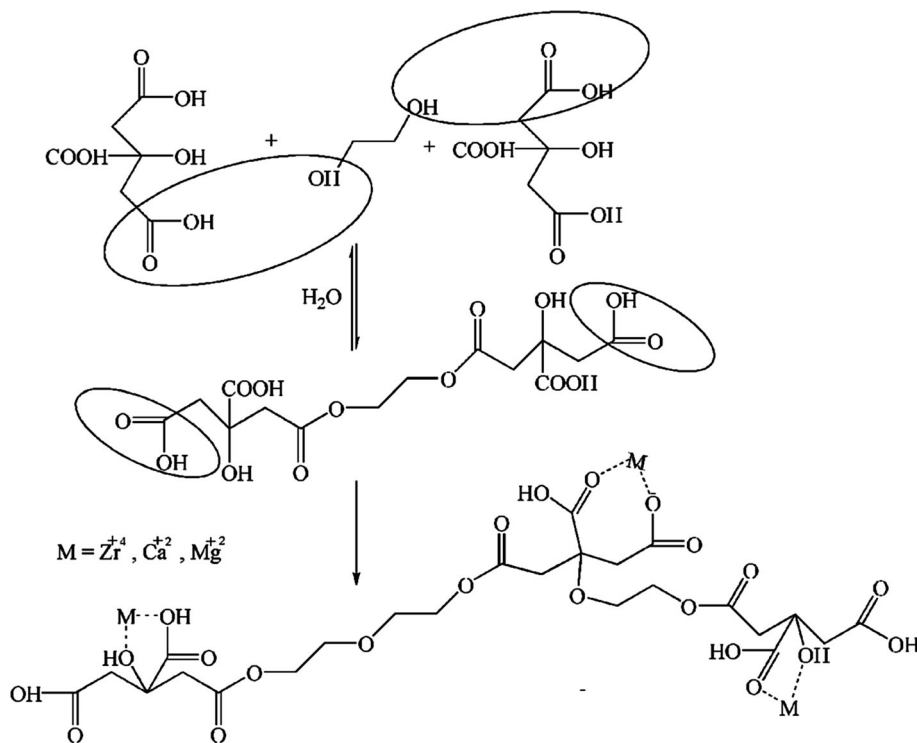


Fig. 5 XRD pattern of synthesized ZrO_2 nanoparticles using sucrose and 20 mL lemon juice

water. The esterification of CA (both free CA and complexed CA) occurs readily in the presence of EG at moderate temperatures ($100\text{--}150\text{ }^\circ\text{C}$), and the prolonged heating of the mixed solution with the concomitant evaporation of excess EG promotes polyesterification, thereby yielding a transparent polymeric resin precursor. The principle underlying this route is, thus, to obtain a polymeric resin precursor comprising randomly branched polymer

Fig. 6 Schematic of esterification of citric acid–ethylene glycol molecules and the distribution of zirconium ions in its polyester



molecules throughout which the zirconium cations are uniformly distributed, as schematically shown in Fig. 6. Heating the polymeric resin at high temperatures (above 300 °C) can cause a breakdown of the polymer. Moreover, in this process, connecting some dissociated carboxylic acid groups (–COO–) through metal ions plays an important role in polymers cross-linking. Thus, although a bonding between a cation and a (dissociated) carboxylic acid group is generally weaker than the chelate bonding in metal–CA complexes, the randomness of the initial solution can be retained in the final polymeric gel. This is because the gel consists of many chains twisted and tangled together, and both cations and solvents are entrapped by the steric hindrance. Due to these tangled chains, the resulting ZrO₂ nanoparticle, after the calcination of the as-obtained gel, was highly agglomerated, as shown in Fig. 1e–d. Figure 1e, f shows that with the addition of sucrose to the starting material, the uniformity of the products was improved. Sucrose is a disaccharide, a molecule derived from two simple monosaccharides (fructose and glucose). In the presence of lemon juice as a catalyst for the hydrolysis of sucrose, this modifier agent was converted to its monomers, i.e., glucose and fructose. It has been reported that in the absence of catalysts, hydrolysis of sucrose is so slow that the solutions of sucrose can sit for years. However, in the acidic medium, such as lemon juice, it can accelerate this conversion (Fig. 7) [29]. Moreover, by heating the solution, the

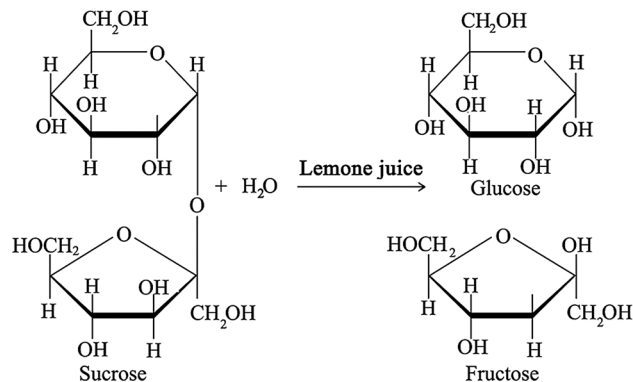


Fig. 7 Schematic illustration of sucrose hydrolysis catalyst by lemon juice

glucose and fructose could be further oxidized into saccharic acid, glycolic acid, and trihydroxy butyric acid, with a large number of –COOH and –OH groups. Furthermore, the COOH groups could be easily coordinated with metal ions in the solution, quite similar to citric acid complexing mechanisms. In this method, sucrose acted as the complexing agent in the synthesis process. Thus, the resulted polymeric resin, in the presence of sucrose, was able to accommodate a higher amount of cations, in comparison with chelating the solution. Also, sucrose was decomposed exothermally at a low ignition temperature (480 °C) [30]. During the calcination of zirconia gel, sucrose, along with hydrolyzed and oxidized products, could be converted to

water and CO₂ gases. These escaping gases caused the better separation of the final nanoparticles. Due to this fact, more uniform ZrO₂ nanoparticles were obtained, as shown in Fig. 1e, f.

3.6 UV–Vis and photoluminescence analysis

ZrO₂ is a direct band gap insulator with two direct band-to-band transitions: 5.2 and 5.79 eV (238 and 214 nm, respectively) [31]. As known, the uppermost molecular orbitals of the valence band (HOMOs) of ZrO₂ are formed by the 2*p* states of oxide ions with some admixing of 4*d* states of Zr⁴⁺; the lowest-energy molecular orbitals of the conduction band (LUMOs) arise from the 4*d* states of Zr⁴⁺ with some admixing of the 2*p* states of oxygen [32]. Figure 8 shows the room temperature UV–VIS absorption spectrum of the synthesized ZrO₂ nanoparticles dispersed in ethanol. A sharp peak observed at about 213 nm (5.82 eV) could be attributed to the band gap energy of [33]. This peak showed a small blue shift compared to the bulk. In the semiconductor nanoparticles, it is usually observed that band gap energy is increased (blue shift) with decreasing particle size [34]. Apart from the strong absorption peak, a weak peak centered at 283 nm (4.2 eV) was observed. As confirmed by EDS and AAS analysis, the Mg⁺² and Ca⁺² were doped in the synthesized nanoparticles, causing a defective structure in these nanoparticles. It has been shown that the high concentration of the dopant ions and compensating anion vacancies results in a wide variety of simple and complex defects in the cation and anion sublattices [35]. Defects associated with anion vacancies dominate in case. This peak was expected to arise from transitions involving extrinsic states such as surface trap states and anion vacancies. Figure 9 shows fluorescence spectrum with an excitation wavelength of 210 nm (5.89 eV). The spectrum features showed a broad band in the range of 310–390 nm, which was followed by a peak at 403 nm with a shoulder of about 411 nm. In

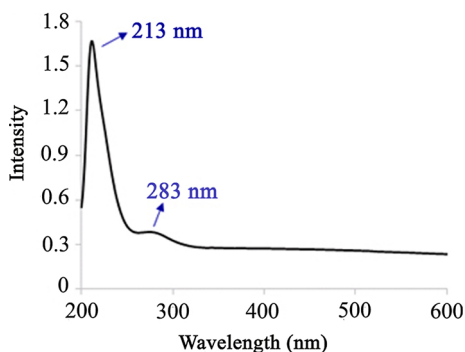


Fig. 8 UV–Vis spectra of ZrO₂ nanoparticles synthesized using 20 mL lemon juice and sucrose

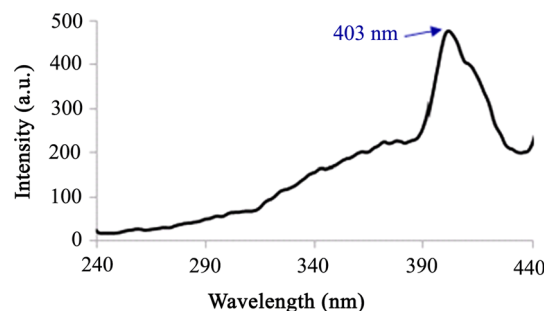


Fig. 9 Photoluminescence spectra of ZrO₂ nanoparticles synthesized using 20 mL lemon juice

general, the emissions that appear at short wavelength can be ascribed to the excitation from the near band-edge transitions [36]. The broad band and the substantial red shift of the band maximum, as compared to the band gap (5.82 eV) of the bulk material, strongly indicated that fluorescence was involved in the mid-gap trap states of ion vacancies.

3.7 FESEM and EDS mapping of the synthesized pellets

The FESEM micrographs of prepared pellets sintered between 1450 and 1700 °C in air atmosphere are shown Fig. 10. The micrographs in Fig. 10 show that prepared pellets except the sample sintered at 1450 °C look comparatively dense, while the grain size was apparently increased as the sintering temperature was increased. It is commonly known that in the final stage of the sintering process where the relative porosity becomes by and large less than 7 %, most of the pores are closed shaped and a ratio of the number of pores to grain becomes constant. In addition, in the final sintering stage, grain growth predominantly occurs rather than a further densification process. From this point of view, all prepared pellets except the sample sintered at 1450 °C have reached the final sintering stage. Moreover, the grain size of the samples showed rather strong dependency at sintering temperatures. As seen from Fig. 10, the grain sizes were distinctly increased as the sintering temperature increases [37]. The densities and grain sizes of as-prepared ZrO₂ samples sintered between 1450 and 1700 °C in air atmosphere are summarized in Table 1, and the relative densities of all samples are not much different except for the sample sintered at 1450 °C because of some existed porosity in its structure.

Figure 11 exhibits EDS mapping analysis of the synthesized ZrO₂ pellet. The results showed that Mg²⁺ and Ca²⁺ elements were uniformly distributed through the whole scanning area, indicating that these cations were

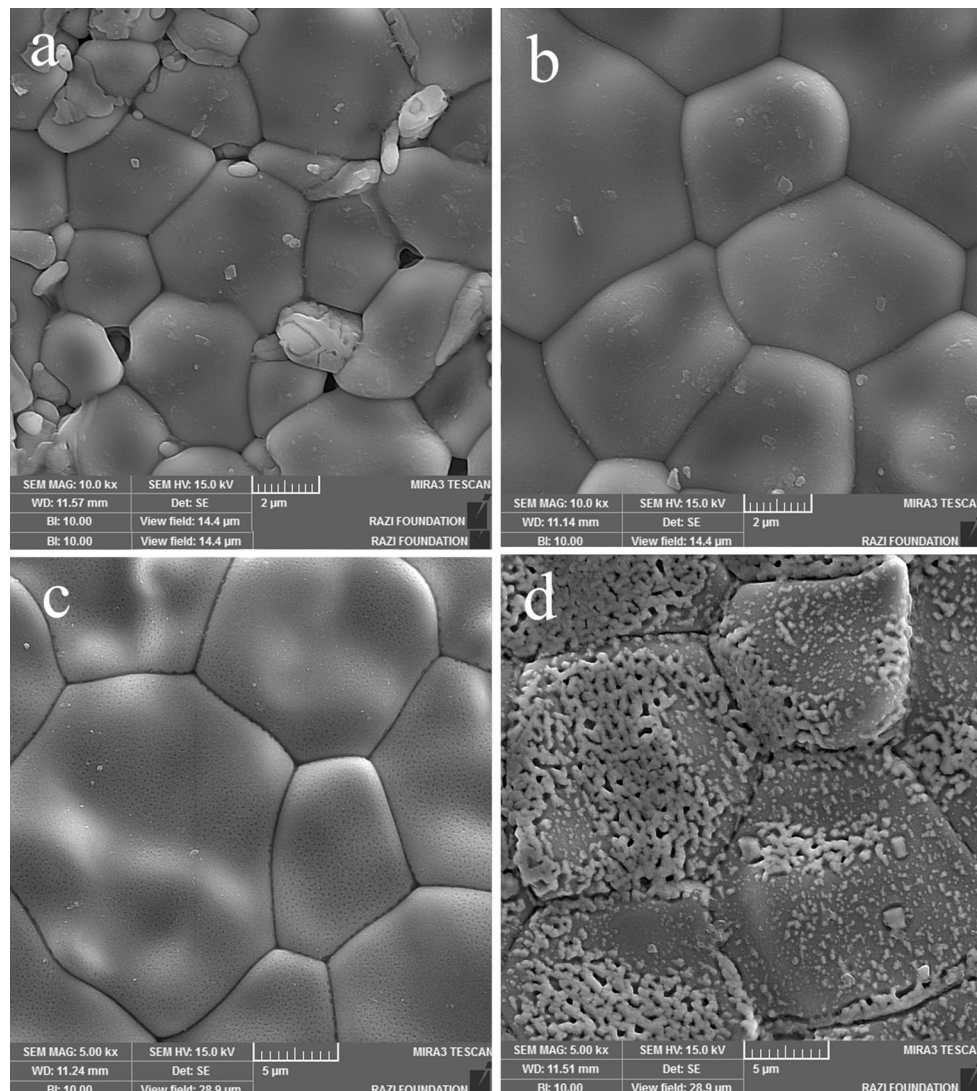


Fig. 10 FESEM images of the prepared pellets at different temperatures **a** 1450 °C, **b** 1550 °C, **c** 1650 °C, and **d** 1700 °C

Table 1 Densities and grain size of the as-prepared pellets at different temperatures

Sample	Sintering temperature (°C)	Density (g/cm ³)	Average grain size (μm)
1	1450	4.79	0.7
2	1550	5.14	5
3	1650	5.31	12
4	1700	5.25	15

uniformly distributed in the ZrO₂ pellet. Table 2 shows the elemental composition of the synthesized pellet. As shown in Table 2, the sample had about 2 wt% Mg and 4.6 wt% Ca in its structure. The good distribution of elements and the dense structure resulted in the good conduction of semiconductor [38, 39]. According to results, the prepared pellets sintered at the 1550 °C that have dense structure and small gain size were selected for conductivity measurements.

3.8 Conductivity measurements

Fuel cell is a device that generates electricity by a chemical reaction of a fuel with oxygen or another oxidizing agent. Fuel cells have traditionally been categorized first by the type of electrolyte and then by the type of fuel used. Fuel cells can be further categorized by the operating temperature, with polymer electrolyte membrane fuel cells (PEMFCs) typically having the lowest operating

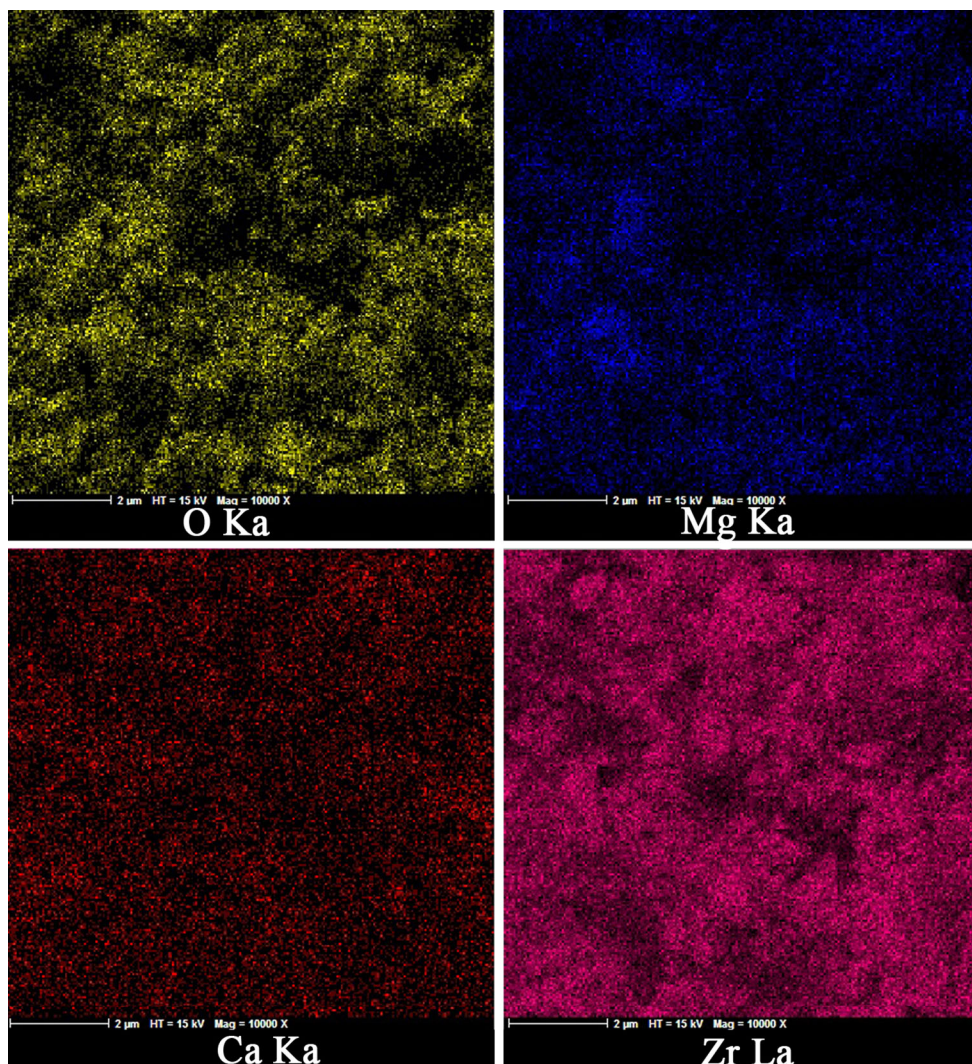


Fig. 11 EDS mapping analysis of Zr, O, Mg, and Ca elements in the synthesized ZrO_2 pellet

Table 2 Elemental composition of the synthesized zirconia pellet

Element	wt%	at. %
Oxygen	27.2	64.7
Magnesium	2.0	3.2
Calcium	4.6	4.4
Zirconium	66.2	27.7
Total	100	100

temperatures, below 100 °C, and SOFCs showing the highest operating temperature, 850–1000 °C. SOFCs have several advantages over other types of fuel cells and are able to convert carbon monoxide as well as hydrogen. Also, at high operating temperatures, fuels can be reformed within the fuel cell itself, eliminating the need for external reforming and allowing the units to be used with a variety of hydrocarbon fuels. They are also relatively resistant to small quantities of sulfur in the fuel. A further advantage of

the high operating temperature is that the reaction kinetics are improved, thereby removing the need for a metal catalyst [40]. However, there are some disadvantages with the high temperature: These cells take longer to start up and reach the operating temperature, they must be constructed of robust, heat-resistant materials that restrict the material selected for the stack components, such as interconnecting and sealing, and they must be shielded to prevent heat loss. Therefore, there is a strong incentive to develop intermediate-temperature solid oxide fuel cells that operate between 500 and 750 °C [41]. The ideal efficiency of fuel cells can be obtained as follows:

$$\eta = \frac{W_{\text{out}}}{Q_{\text{in}}} = \frac{\Delta G}{\text{HHV}} = \frac{nFE}{\text{HHV}},$$

where work done (W_{out}) is given by ΔG (or nFE) and heat input (Q_{in}) is calculated based upon the higher heating value of fuel. But the ideal and actual performance of a fuel

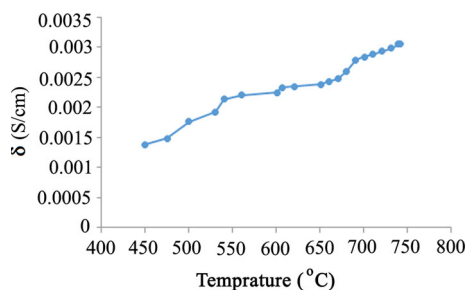


Fig. 12 Electrical conductivity of synthesized ZrO₂ pellet

cell is quite different, and the actual cell potential is lower than its equilibrium potential because of irreversible losses due to various reasons. The losses, which are generally called polarization or overpotential, originate primarily from activation polarization, ohmic polarization, and gas concentration polarization. Ohmic losses in fuel cells mainly result from ionic conductivity through the electrolyte [42]. One way to reduce ohmic resistance in SOFCs is operating at higher temperatures. The ionic conductivity of the solid oxide is defined as follows [43]:

$$\sigma = \sigma_0 \cdot e^{\frac{-E}{RT}},$$

where σ_0 and E factors depend on electrolyte materials, T is the electrolyte temperature, and R is the ideal gas constant. So, by decreasing the operating temperature of solid oxide fuel cells (SOFCs), the ionic conductivity is decreased. On the other hand, the electrolyte conductivity is also closely related to the starting powder. The electrical conductivity in an oxide can be related to the type and concentration of the dopants and the microstructure [44]. The electrical conductivity of a solid electrolyte is explained by the so-called brick layer model [45]. This model shows that grain boundaries have a lower effective charge carrier concentration and are more resistive than the grains. The magnitude of grain boundary conductivity is almost twice less than that of the grain conductivity. Experimental studies on fully dense, highly pure specimens of nano- and microcrystalline, different ions-doped zirconia have shown a significant increase in the conductivity at interfaces with decreasing crystallite size to nanometer [46]. Figure 12 displays the ionic conductivity as a function of temperature. The electrical conductivity of the sample reached 0.0034 S/cm at 750 °C. For oxygen ion transport in based electrolytes, the charge carriers were oxygen vacancies. The following equation is usually applied to oxygen ionic conductors [47]:

$$\text{Log}(\sigma T) = \text{log} A - \frac{E_a}{2.303k_B T},$$

where σ is the ionic conductivity, T is the absolute temperature, A is the pre-exponential constant, and E_a is the

activation energy. The activation energy normally includes energy terms of the formation and migration of oxygen vacancies. In the extrinsic regime, the activation energy is dominated by the migration energy. In this case, the activation energy could be represented by the migration energy for the doped oxide ionic conductors in the extrinsic regime. The conductivity data were fitted to the above equation by a least square analysis. The correlation factor of the linear regression for the above equation was 0.982. The conductivity activation energy of 31.015 kJ/mol was observed for this sample. The results revealed that this cubic nanoparticle could have fairly good electrical properties, with a potential application as an electrolyte material in intermediate-temperature solid oxide fuel cells (IT-SOFCs).

4 Summary and conclusion

To summarize, ZrO₂ nanoparticles were successfully prepared via a green method using lemon juice at the ambient temperature. The results showed that sucrose addition protected the synthesized particles from aggregation. SEM images also showed that the sample prepared with 20 mL lemon juice and sucrose had the smaller particle size of 20 nm, as compared to other samples. Furthermore, the XRD results showed the cubic-phase formation of the prepared ZrO₂ nanoparticles. EDS analysis for ZrO₂ prepared by 20 mL lemon juice and sucrose revealed that Ca and Mg existed in ZrO₂ structure. The UV–Vis and PL spectra indicated that the particles had a narrow size with extrinsic states. This sample was chosen, and a cubic pellet was prepared by sintering the sample. Overall, it was verified that ZrO₂ nanoparticles synthesized with this method could be one of the promising electrolyte materials for intermediate- or low-temperature SOFCs.

Acknowledgments We are grateful to the University of Tehran for the financial support. We also appreciate the contribution from the Research Council of Isfahan University of Technology (IUT).

References

1. Zink N et al (2013) Low temperature synthesis of monodisperse nanoscaled ZrO₂ with a large specific surface area. *Dalton Trans* 42:432
2. Davar F, Hassankhani A, Loghman-Estarki MR (2013) Controllable synthesis of metastable tetragonal zirconia nanocrystals using citric acid assisted sol–gel method. *Ceram Int* 39:2933–2941
3. Loghman-Estarki MR et al (2013) Comparative studies on synthesis of nanocrystalline Sc₂O₃–Y₂O₃ doped zirconia (SYDZ) and YSZ solid solution via modified and classic Pechini method. *CrystEngComm* 15:5898
4. Loghman-Estarki MR, Nejati M, Edris H, Razavi RS, Jamai H (2015) Evaluation of hot corrosion behavior of plasma sprayed

- scandia and yttria co-stabilized nanostructured thermal barrier coatings in the presence of molten sulfate and vanadate salt. *J Eur Ceram Soc* 35:693–702
5. Tsunekawa S et al (2003) Critical size of the phase transition from cubic to tetragonal in pure zirconia nanoparticles. *Nano Lett* 3:871
 6. Serena S, Caballero A, Sainz MA (2013) Analysis of the polymorphic transformation of nano- and microcrystalline zirconia doped with CaO and MgO during reaction-sintering process by neutron thermodiffraction. A thermodynamic approach. *J Eur Ceram Soc* 33:1413
 7. Nath S, Sinha N, Basu B (2008) Microstructure, mechanical and tribological properties of microwave sintered calcia-doped zirconia for biomedical applications. *Ceram Int* 34:1509
 8. Flegler AJ et al (2014) Cubic yttria stabilized zirconia sintering additive impacts: a comparative study. *Ceram Int* 40:16323
 9. Petrik NG, Taylor DP, Orlando TM (1999) Laser-stimulated luminescence of yttria-stabilized cubic zirconia crystals. *J Appl Phys* 85:6770
 10. Tan D et al (2009) Preparation of zirconia nanoparticles by pulsed laser ablation in liquid. *Chem Lett* 38:1102
 11. Brossmann U et al (2007) Microwave plasma synthesis of nano-crystalline YSZ. *Phys Status Solidi (RRL) Rapid Res Lett* 1:107
 12. Salavati-Niasari M, Dadkhah M, Davar F (2009) Pure cubic ZrO₂ nanoparticles by thermolysis of a new precursor. *Polyhedron* 28:3005
 13. Meetei SD, Singh SD (2014) Hydrothermal synthesis and white light emission of cubic ZrO₂:Eu³⁺ nanocrystals. *J Alloys Compd* 587:143
 14. Majedi A, Davar F, Abbasi A (2014) Sucrose-mediated sol–gel synthesis of nanosized pure and S-doped zirconia and its catalytic activity for the synthesis of acetyl salicylic acid. *J Ind Eng Chem* 20:4215
 15. Barrera-Solano C et al (1994) Obtaining and sintering yttria stabilized zirconia (YSZ) powders from alkoxides. *J Sol-Gel Sci Technol* 2:347
 16. Răileanu M et al (2015) Sol-gel zirconia-based nanopowders with potential applications for sensors. *Ceram Int* 41:4381
 17. Liu Y et al (2012) Amine-functionalized lanthanide-doped zirconia nanoparticles: optical spectroscopy, time-resolved fluorescence resonance energy transfer biodetection, and targeted imaging. *J Am Chem Soc* 134:15083
 18. Hench LL, West JK (1990) The sol-gel process. *Chem Rev* 90:33
 19. Lin C, Zhang C, Lin J (2007) Phase transformation and photoluminescence properties of nanocrystalline ZrO₂ powders prepared via the Pechini-type sol–gel process. *J Phys Chem C* 111:3300
 20. Razpotnik T, Maček J (2007) Synthesis of nickel oxide/zirconia powders via a modified Pechini method. *J Eur Ceram Soc* 27:1405
 21. Laberty-Robert C et al (2002) Synthesis of YSZ powders by the sol-gel method: surfactant effects on the morphology. *Solid State Sci* 4:1053
 22. Kumar PPNV et al (2014) Green synthesis and characterization of silver nanoparticles using *Boerhaavia diffusa* plant extract and their anti bacterial activity. *Ind Crops Prod* 52:562
 23. Bala N et al (2015) Green synthesis of zinc oxide nanoparticles using *Hibiscus subdariffa* leaf extract: effect of temperature on synthesis, anti-bacterial activity and anti-diabetic activity. *RSC Adv* 5:4993
 24. Lorente J et al (2014) Chemical guide parameters for Spanish lemon (*Citrus limon* (L.) Burm.) juices. *Food Chem* 162:186
 25. Dimri MC et al (2012) Room-temperature ferromagnetism in Ca and Mg stabilized cubic zirconia bulk samples and thin films prepared by pulsed laser deposition. *J Phys D Appl Phys* 45:475003
 26. Singh KA, Pathak LC, Roy SK (2007) Effect of citric acid on the synthesis of nano-crystalline yttria stabilized zirconia powders by nitrate–citrate process. *Ceram Int* 33:1463
 27. Guo G-Y, Chen Y-L (2001) High-quality zirconia powder resulting from the attempted separation of acetic acid from acrylic acid with zirconium oxychloride. *J Mater Chem* 11:1283
 28. Sarkar D et al (2007) Synthesis and characterization of sol–gel derived ZrO₂ doped Al₂O₃ nanopowder. *Ceram Int* 33:1275
 29. Dawber JG, Brown DR, Reed RA (1966) Acid-catalyzed hydrolysis of sucrose: a student study of a reaction mechanism. *J Chem Educ* 43:34
 30. Joseph AM (1989) Thermal decomposition of carbohydrates, in thermal generation of aromas. American Chemical Society, Washington, p 32
 31. Sahu HR, Rao GR (2000) Characterization of combustion synthesized zirconia powder by UV–vis, IR and other techniques. *Bull Mater Sci* 23:349
 32. Emeline A et al (1998) Spectroscopic and photoluminescence studies of a wide band gap insulating material: powdered and Colloidal ZrO₂ sols. *Langmuir* 14:5011
 33. Xu X, Wang X (2009) Fine tuning of the sizes and phases of ZrO₂ nanocrystals. *Nano Res* 2:891
 34. Reddy KM, Manorama SV, Reddy AR (2003) Bandgap studies on anatase titanium dioxide nanoparticles. *Mater Chem Phys* 78:239
 35. Choi S-I, Takeuchi T (1983) Electronic states of F-type centers in oxide crystals: a new picture. *Phys Rev Lett* 50:1474
 36. Liang J et al (2002) Photoluminescence of tetragonal ZrO₂ nanoparticles synthesized by microwave irradiation. *Inorg Chem* 41:3602
 37. Lee DS et al (2005) Characterization of ZrO₂ co-doped with Sc₂O₃ and CeO₂ electrolyte for the application of intermediate temperature SOFCs. *Solid State Ion* 176:33
 38. Yao M et al (2014) The influence of titanium doping on the electric properties of amorphous alumina films prepared by sol–gel technology. *J Sol-Gel Sci Technol* 74:39
 39. Kulkarni S, Duttgupta S, Phatak G (2014) Sol–gel synthesis and protonic conductivity of yttrium doped barium cerate. *J Sol-Gel Sci Technol* 74:94
 40. Kilner JA, Burriel M (2014) Materials for intermediate-temperature solid-oxide fuel cells. *Annu Rev Mater Res* 44:365
 41. Shao Z, Zhou W, Zhu Z (2012) Advanced synthesis of materials for intermediate-temperature solid oxide fuel cells. *Prog Mater Sci* 57:804
 42. Rayment C, Sherwin S (2003) Introduction to fuel cell technology. Department of Aerospace and Mechanical Engineering, University of Notre Dame, Notre Dame, p 1
 43. Milewski J, Miller A (2006) Influences of the type and thickness of electrolyte on solid oxide fuel cell hybrid system performance. *J Fuel Cell Sci Technol* 3:396
 44. Kumar B et al (2005) Electrical properties of heterogeneously doped yttria stabilized zirconia. *J Power Sources* 140:12
 45. Guo X, Ding Y (2004) Grain boundary space charge effect in zirconia: experimental evidence. *J Electrochem Soc* 151:J1
 46. Mondal P et al (1999) Enhanced specific grain boundary conductivity in nanocrystalline Y₂O₃-stabilized zirconia. *Solid State Ion* 118:331
 47. Hui S et al (2007) A brief review of the ionic conductivity enhancement for selected oxide electrolytes. *J Power Sources* 172:493